Title
Retinoid X Receptor Activation Alters the Chromatin Landscape To Commit Mesenchymal Stem Cells to the Adipose Lineage.

Journal
Endocrinology, 158(10)

ISSN
0013-7227

Authors
Shoucri, Bassem M
Martinez, Eric S
Abreo, Timothy J
et al.

Publication Date
2017-10-01

DOI
10.1210/en.2017-00348

Retinoid X Receptor Activation Alters the Chromatin Landscape To Commit Mesenchymal Stem Cells to the Adipose Lineage

Bassem M. Shoucri,[1,2] Eric S. Martinez,[1] Timothy J. Abreo,[1] Victor T. Hung,[1] Zdena Moosova,[1,3] Toshi Shioda,[4] and Bruce Blumberg[1,5]

[1]Department of Developmental and Cell Biology, University of California, Irvine, Irvine, California 92697-2300; [2]Medical Scientist Training Program, University of California, Irvine, Irvine, California 92697; [3]Masaryk University, Faculty of Science, RECETOX, 625 00 Brno, Czech Republic; [4]Massachusetts General Hospital Center for Cancer Research and Harvard Medical School, Charlestown, Massachusetts 02129; and [5]Department of Pharmaceutical Sciences, University of California, Irvine, Irvine, California 92697

Developmental exposure to environmental factors has been linked to obesity risk later in life. Nuclear receptors are molecular sensors that play critical roles during development and, as such, are prime candidates to explain the developmental programming of disease risk by environmental chemicals. We have previously characterized the obesogen tributyltin (TBT), which activates the nuclear receptors peroxisome proliferator-activated receptor γ (PPARγ) and retinoid X receptor (RXR) to increase adiposity in mice exposed *in utero*. Mesenchymal stem cells (MSCs) from these mice are biased toward the adipose lineage at the expense of the osteoblast lineage, and MSCs exposed to TBT *in vitro* are shunted toward the adipose fate in a PPARγ-dependent fashion. To address where in the adipogenic cascade TBT acts, we developed an *in vitro* commitment assay that permitted us to distinguish early commitment to the adipose lineage from subsequent differentiation. TBT and RXR activators (rexinoids) had potent effects in committing MSCs to the adipose lineage, whereas the strong PPARγ activator rosiglitazone was inactive. We show that activation of RXR is sufficient for adipogenic commitment and that rexinoids act through RXR to alter the transcriptome in a manner favoring adipogenic commitment. RXR activation alters expression of enhancer of zeste homolog 2 (EZH2) and modifies genome-wide histone 3 lysine 27 trimethylation (H3K27me3) in promoting adipose commitment and programming subsequent differentiation. These data offer insights into the roles of RXR and EZH2 in MSC lineage specification and shed light on how endocrine-disrupting chemicals such as TBT can reprogram stem cell fate. **(*Endocrinology* 158: 3109–3125, 2017)**

Thirty eight percent of American adults are obese, as are 17% of US children (1, 2). The obese population is at risk for a number of comorbidities, including cardiovascular disease, type 2 diabetes, hypertension, and many cancers. This comes at a tremendous cost to the US economy, estimated to be >$200 billion annually (3). Clinical management of obesity remains focused on lifestyle modification in obese and overweight adults (4, 5). However, substantial evidence shows that environmental factors *in utero* and in early life have a profound effect on human health in adulthood (6). In particular, exposure to xenobiotic chemicals during early development has been implicated as an important contributor to the obesity epidemic (7–9).

ISSN Print 0013-7227 ISSN Online 1945-7170
Printed in USA

Received 11 April 2017. Accepted 11 July 2017.
First Published Online 14 July 2017

Abbreviations: ChIP, chromatin immunoprecipitation; DEG, differentially expressed gene; DMSO, dimethyl sulfoxide; DZNep, 3-deazaneplanocin; EDC, endocrine-disrupting chemical; ES, embryonic stem; EZH2, enhancer of zeste homolog 2; GO, gene ontology; H3K27me3, histone 3 lysine 27 trimethylation; LXR, liver X receptor; MDI, isobutylmethylxanthine, dexamethasone, and insulin; MSC, mesenchymal stem cell; PPAR, peroxisome proliferator-activated receptor; PRC2, Polycomb repressive complex 2; qPCR, quantitative polymerase chain reaction; RAR, retinoic acid receptor; RNA-seq, RNA sequencing; ROSI, rosiglitazone; RXR, retinoid X receptor; shRNA, short hairpin RNA; TBT, tributyltin; TTNPB, arotinoid acid.

Our group proposed the obesogen hypothesis, which holds that exposure to exogenous chemicals during development can increase risk of obesity later in life (10). Results from many laboratories support and extend this hypothesis in humans and animal models (reviewed in 7, 9, 11). Although the mechanisms of action for most obesogens are unclear, many obesogens are known to act through nuclear receptors to promote the development of fat tissue (reviewed in 9, 11, 12).

Adipogenesis in humans and mice begins *in utero* and continues during the postnatal period (13–15). Transformation of a mesenchymal stem cell (MSC; also known as multipotent stromal cell) into a white adipocyte requires initial commitment to the adipose lineage, followed by terminal differentiation into a mature adipocyte (16). The goal of adipose lineage commitment is to induce expression of the master regulator of adipogenesis, the nuclear receptor peroxisome proliferator-activated receptor γ (PPARγ), which is both necessary and sufficient to stimulate terminal differentiation (17).

We and others demonstrated that tributyltin (TBT) acts through the nuclear receptor PPARγ and its heterodimeric partner retinoid X receptor (RXR) to promote adipogenesis and alter lipid homeostasis *in vitro* and *in vivo* (18, 19). Mice exposed to nanomolar levels of TBT *in utero* display increased lipid accumulation in adipose depots, livers, and testis as adults, and MSCs from these animals are reprogrammed to favor the adipose lineage at the expense of the osteogenic lineage (18, 20, 21). The effects of TBT are transgenerational and can be detected in the F1, F2, and F3 descendants of F0 mice exposed during pregnancy (20). In a standard *in vitro* adipogenesis assay, human and mouse MSCs or 3T3-L1 preadipocytes exposed to TBT or the PPARγ agonist rosiglitazone (ROSI) are shunted toward the adipocyte lineage via a PPARγ-dependent pathway (21, 22). These studies did not address precisely where in the adipogenic pathway TBT acted to promote both lineage commitment and adipogenic differentiation.

One limitation within the adipogenesis field is the widespread use of the 3T3-L1 cell line, which is already committed to the adipose lineage. Primary bone marrow–derived MSCs offer an attractive alternative to these cells because they are easy to obtain and culture, but allow for the study of lineage commitment *in vitro*. They also offer a viable platform to screen endocrine-disrupting chemicals (EDCs) and study their mechanisms of action in a dish. A further limitation of current *in vitro* methods is the use of adipose induction cocktails whose components both commit and differentiate MSCs into adipocytes. Therefore, it is impossible to decipher whether a chemical of interest, such as TBT, acts during one or both of these phases of development because chemicals are added in conjunction with the induction cocktail. One *in vitro* model that has effectively separated commitment and differentiation is the MSC-like cell line C3H10T1/2. These cells can be committed to the adipose lineage by pretreatment with bone morphogenetic protein 4 or an inhibitor of DNA methylation prior to differentiation with a standard adipogenic cocktail [isobutylmethylxanthine, dexamethasone, and insulin (MDI)] (23–25). No such system has been established for primary MSCs.

Because both prenatal TBT and ROSI treatment increased the number of preadipocytes *in vivo* in F1 animals treated *in utero* (21), but only TBT could elicit transgenerational effects on adipogenic commitment of MSCs in F3 descendants of F0-treated animals (20), we hypothesized that there was some fundamental difference in how ROSI and TBT acted during MSC commitment and/or differentiation. To test this hypothesis, we developed an *in vitro* commitment assay that allowed us to distinguish between effects on adipogenic commitment and differentiation by pretreating MSCs with candidate chemicals for 48 hours prior to differentiating them with the adipogenic cocktail. Surprisingly, a 2-day pretreatment with TBT prior to adipose induction resulted in as much lipid accumulation as the standard 2-week adipogenesis assay cotreatment. Although ROSI is a potent inducer of adipogenesis, it was unable to commit MSCs to the adipogenic lineage in our commitment assay. We infer that TBT induces adipose lineage commitment in a RXR-dependent, PPARγ-independent manner.

RXR has long been considered indispensable for adipose differentiation due to the critical heterodimer it forms with the master regulator of adipogenesis, PPARγ (26, 27). Transcriptomal analyses of MSCs revealed genome-wide changes in transcription that were induced by TBT or the RXR-selective agonist, IRX4204, but not the strong PPARγ agonist, ROSI. Furthermore, we found that RXR activation reduced the expression of the repressive histone modifier enhancer of zeste homolog 2 (EZH2), resulting in a genome-wide redistribution and overall decrease of repressive H3K27me3 marks, particularly near key adipogenic regulators. These data identify RXR as an environmental sensor that can alter epigenomic architecture to influence lineage allocation of the MSC compartment during development.

Materials and Methods

Chemicals

TBT, ROSI (Cayman Chemical, Ann Arbor, MI), IRX4204 (also known as AGN194204; a gift of Rosh Chandraratna, IO Therapeutics, Santa Ana, CA), T0070907 (Enzo Life Sciences, Farmingdale, NY), HX531 (a gift of Claes Bavik, Acucela,

Seattle, WA), LG100268, 9-*cis* retinoic acid (Enzo Life Sciences), all-*trans* retinoic acid, TTNPB, WY14643, GW501516, GW3965, 3-deazaneplanocin (DZNep) (ApexBio, Houston, TX), dexamethasone, insulin, isobutylmethylxanthine, ascorbic acid 2-phsophate, β-glycerolphosphate, formaldehyde (Thermo Fisher Scientific, Waltham, MA), Nile Red, Hoechst 33342, polybrene, and puromycin were purchased from Sigma-Aldrich (St. Louis, MO), unless otherwise indicated.

Cell culture, chemical treatment

Bone marrow–derived multipotent MSCs from the long bones of C57BL/6J mice (MSCs) were purchased at passage 6 (OriCell; Cyagen Biosciences, Santa Clara, CA) and stored at passage 8 or 9 in liquid N2. Cells were maintained, as previously described (28), in Dulbecco's modified Eagle medium containing 10% calf bovine serum, 10 mM HEPES, 1 mM sodium pyruvate, 100 IU/mL penicillin, and 100 μg/mL streptomycin. MSCs were plated at 15,000 cells/cm^2 in 24-well, 12-well, or 10-cm plates. For standard adipogenesis assays [Fig. 1(a)], cells were maintained in media without any treatment until confluent after 72 hours. For commitment assays [Fig. 1(a)], cells were allowed to attach and acclimate for 24 hours prior to 48 hours of chemical treatment (day −2 through day 0). After 48 hours (day 0), MSCs were confluent and ready for differentiation. Due to its short half-life, the PPARγ antagonist T0070907 was dosed every 12 hours during pretreatment (22). The amount of dimethyl sulfoxide (DMSO) vehicle was kept at <0.1% in all assays.

Adipose/bone differentiation and staining

At confluency, cells were differentiated in minimal essential medium α containing 15% fetal bovine serum, 10 mM HEPES, 2 mM L-glutamine, 100 IU/mL penicillin, and 100 μg/mL streptomycin, supplemented with an adipose induction cocktail [500 μM isobutylmethylxanthine, 1 μM dexamethasone, 5 μg/mL insulin (MDI)] or an osteogenic induction cocktail (10 nM dexamethasone, 50 μM ascorbic acid 2-phosphate, and 10 mM β-glycerophosphate). Media was changed every 3 to 4 days for 14 days prior to fixation in 3.7% formaldehyde. Neutral lipids were stained with Nile Red (1 μg/mL), and nucleic acid was stained with Hoechst 33342 (1 μg/mL). Total fluorescence per well was measured in a SpectraMax Gemini XS spectrofluorometer (Molecular Devices, Sunnyvale, CA) using SoftMax Pro (Molecular Devices); Nile Red relative fluorescence units (RFU) were normalized to Hoechst RFU for each well. Cells were imaged by confocal microscopy on a Zeiss LSM 700 (Zeiss, Oberkochen, Germany) and processed using Volocity (PerkinElmer, Waltham, MA) at the University of California Irvine Optical Biology Core.

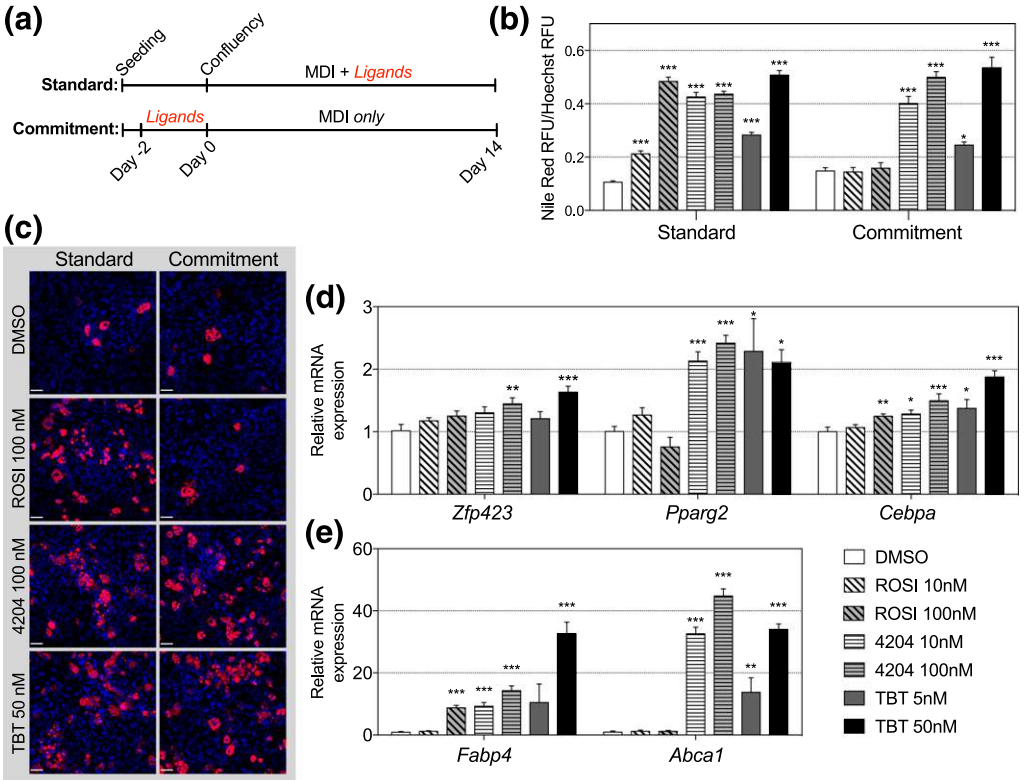

Figure 1. MSCs pretreated with TBT and RXR agonist, but not PPARγ agonist, accumulate more lipid during subsequent adipose differentiation. Mouse bone marrow–derived MSCs were pretreated with vehicle control (0.05% DMSO), ROSI (10, 100 nM), 4204 (10, 100 nM), or TBT (5, 50 nM) for 48 hours prior to induction with an adipose induction cocktail (MDI) for 2 weeks. (a) This commitment assay was run in parallel with a standard 2-week adipogenesis assay, whereby chemical ligands were added in conjunction with MDI. (b) After 14 days of adipose induction, MSCs were fixed and then stained with Nile Red and Hoechst 33342 for lipid and nucleic acid content, respectively. Nile Red relative fluorescence units (RFU) were normalized to Hoechst RFU. (c) Cells were imaged by confocal fluorescence microscopy. Scale bar = 55 μm. (d) Expression of early adipose lineage markers was assessed at day 0 by qPCR. (e) Expression of canonical PPARγ and RXR targets was also analyzed by qPCR at day 0. Data are represented as mean ± standard error of the mean; one-way analysis of variance, Dunnett test; *$P < 0.05$; **$P < 0.01$; ***$P < 0.001$.

Lentiviral transduction

Hairpin-pLKO plasmids [RNAi Consortium short hairpin RNA (shRNA) Library, TRC/Broad Institute, Cambridge, MA] along with packaging and envelope plasmids were transfected into 293T packaging cells, as previously described (see http://portals.broadinstitute.org/gpp/public/). MSCs were seeded at 20,000 cells per well in six-well plates (2000 cells/cm^2). After 24 hours, cells were transduced overnight in 1 mL antibiotic-free media with 8 μg/mL polybrene and 50 μL high titer lentivirus expressing vector alone (pLKO.1) or shRNA against messenger RNA targets (Supplemental Table 1). Following transduction, MSCs were allowed to recover in fresh media (with antibiotics) for 24 hours prior to a 48-hour selection with 2 μg/μL puromycin. Successfully transduced cells were expanded and frozen for further assaying.

RNA isolation, reverse transcription, quantitative polymerase chain reaction

Cells were lysed with TriPure (Roche, Basel, Switzerland) and total RNA isolated with MiniPrep columns (Zymo Research, Irvine, CA). Complementary DNA was generated from 1 μg total RNA using transcriptor reverse transcription (Roche), according to the manufacturer's protocol. Real-time quantitative polymerase chain reaction (qPCR) was conducted on a Roche LightCycler 480 II (Roche) using FastStart SYBR Green Master Mix (Roche) and intron-spanning primers (Supplemental Table 1). Cycle threshold values were calculated as the second derivative maximum in LightCycler software (Roche). Relative quantification and error propagation were performed using the $2^{-\Delta\Delta Ct}$ method, as previously described (29).

Chromatin immunoprecipitation

Chromatin immunoprecipitation (ChIP) was performed as previously described (30), with slight modifications. MSCs were plated and treated in 10-cm plates. At the end of chemical treatment (day 0), cells were fixed at room temperature for 10 minutes with 1% paraformaldehyde (Ted Pella, Redding, CA) in unsupplemented Dulbecco's modified Eagle medium, washed with ice-cold phosphate-buffered saline, then quenched for 5 minutes with 125 mM glycine. Fixed cells were washed, scraped from plates, centrifuged, and then resuspended in 1 mL phosphate-buffered saline/10^7 cells. Equal numbers of cells were spun down, flash frozen in liquid N2, and stored at −80°C. To isolate nuclei, cell pellets were lysed at 4°C for 10 minutes with mild detergents (50 mM HEPES-KOH, pH 7.5, 140 mM NaCl, 1 mM EDTA, 10% glycerol, 0.5% Nonidet P-40, 0.25% Triton X-100, protease inhibitors). Nuclei were spun down, washed for 10 minutes at room temperature (10 mM Tris-HCl, pH 8.0, 200 mM NaCl, 1 mM EDTA, 0.5 mM EGTA, protease inhibitors), and finally lysed in 300 μL nuclear lysis buffer (10 mM Tris-HCl, pH 8.0, 200 mM NaCl, 1 mM EDTA, 0.5 mM EGTA, 0.1% Na-deoxycholate, 0.5% *N*-lauroylsarcosine, protease inhibitors). Chromatin was sonicated in 0.5 mL thin-walled polymerase chain reaction tubes (BrandTech, Essex, CT) using a QSonica Q800R2 (QSonica, Newtown, CT) with the following settings: 30 minutes, 30 seconds on/30 seconds off, amplitude 40%. One percent Triton X-100 was added to sonicated lysate prior to high-speed, cold centrifugation to remove debris. A total of 5 μg DNA was immunoprecipitated with preblocked protein A/G Dynabeads (Thermo Fisher Scientific) complexed to 2.5 μg antibody (anti-H3K4me3, ab8580, RRID:AB_306649, Abcam, Cambridge, UK; anti–histone 3 lysine 27 trimethylation (anti-H3K27me3), ab6002, RRID: AB_305237, Abcam). Beads were washed four times with LiCl buffer (50 mM HEPES-KOH, pH 7.5, 500 mM LiCl, 1 mM EDTA, 1% Nonidet P-40, 0.7% Na-deoxycholate) and once with Tris-EDTA buffer plus 50 mM NaCl. Beads were resuspended in elution buffer (50 mM Tris-HCl, pH 8.0, 10 mM EDTA, 1% sodium dodecyl sulfate) and incubated at 65°C for 30 minutes to release chromatin from beads. Eluate and input controls were reverse cross-linked overnight at 65°C. DNA was isolated using the Zmyo ChIP DNA Clean & Concentrator kit (Zymo Research) following RNase A (0.2 mg/mL, 2 hours, 37°C) and proteinase K (0.2 mg/mL, 2 hours, 55°C) treatment. Input DNA content was determined by Nanodrop (Thermo Fisher Scientific).

Deep sequencing

Integrity of total RNA was evaluated using Tapestation high-sensitivity RNA screen tapes (Agilent Technologies, Santa Clara, CA). Range of the RNA integrity number was 8.0 to 8.6. Strand-specific, barcode-indexed RNA sequencing (RNA-seq) deep-sequencing libraries were synthesized from total RNA with ERCC spike-in controls (Thermo Fisher Scientific) using Ovation RNA-Seq Systems 1-16 for Mouse (NuGen Technologies, San Carlos, CA). Size distribution of the libraries was determined by Tapestation to be 200 to 800 bp, peaking at 300 bp. RNA-seq libraries were quantified using KAPA Illumina library quantification kit (KAPA Biosystems, Wilmington, MA), and up to 12 libraries were pooled in each run of the Illumina NextSeq500 deep sequencer (75 nt + 75 nt, paired-end) to generate fastq raw read sequence files.

Size distribution of ChIP-enriched genomic DNA fragments was evaluated using D1000 high-sensitivity DNA screen tape to be 100 to 300 bp, peaking at ~200 bp. ChIP-seq deep-sequencing libraries were synthesized using NEBNext Ultra Library Prep Kit (New England Biolabs, Ipswich, MA). Libraries were subjected to size distribution analysis using Tapestation (125 bp to 300 bp, peaking at 200 bp) and quantified using the KAPA kit to pool up for NextSeq500 sequencing (75 nt, single) to generate fastq data.

Deep-sequencing data analysis

RNA-Seq and ChIP-Seq deep-sequencing reads (fastq data) were aligned to the mouse genome reference sequence GRCm38/mm10 using the STAR aligner (31), and the resulting bam format aligned reads were subjected to QC analysis using fastQC (Babraham Institute, Cambridge, United Kingdom; http://www.bioinformatics.babraham.ac.uk/projects/fastqc/), followed by extraction of uniquely mapped reads using samtools (32). Depth of deep sequencing of each sample is summarized as uniquely mapped read numbers in Supplemental Table 2. For RNA-seq data analysis, uniquely mapped reads were assigned to the mm10 gene model and on-exon reads were counted using Bioconductor package "Rsubread" (33). The assigned read counts were normalized using Bioconductor package "DESeq2" (34). Differential expression was assessed in DESeq2 using the DESeq function with $\alpha = 0.01$. Differentially expressed genes (DEGs) were defined by Benjamini–Hochberg corrected P values (p-adj < 0.01) and fold change [absolute value of $\log_2$ (fold change) > 0.2]. Hierarchical clustering was performed on the most differentially expressed genes using Cluster 3.0 and visualized in Java TreeView. For gene ontology (GO) term and pathway analysis, DEGs were converted to

HUGO gene symbols, and then tested for enrichment in MSigDB (Broad Institute) pathway (c2) and GO term (c5) gene sets by hypergeometric test in R. *P* values were corrected for multiple testing using the Benjamini–Hochberg method.

For ChIP-seq data, from the bam file data of uniquely mapped reads, genomic regions enriched with H3K4me3 or H3K27me3 histone marks were detected using spatial clustering for identification of ChIP-enriched regions (SICER) (35) with the following arguments: W = 200, G = 600, false discovery rate cutoff = 0.001. The output BED files of SICER were then subjected to detection of differential enrichment of the histone marks using Bioconductor package "DiffBind" with the default parameters of function dba.analyze (36). Data were visualized using Bioconductor package "ChIPseeker" (37). Genomic regions showing significant differential enrichment of the histone marks were annotated to nearby genes using Genomic Regions Enrichment of Annotations Tool (38) with 5 kb upstream, 1 kb downstream, and 1 Mb distal search parameters. GO term and pathway analyses were conducted on annotated genes, as described previously.

All sequencing data are available on the Gene Expression Omnibus (GSE99565).

Statistical analysis

Data visualization and statistical analyses were conducted in Prism 7 (GraphPad Software, La Jolla, CA), excluding much of the genomic analyses that were completed in R and other software packages, as noted earlier. Four to six biological replicates were used for all experiments. Errors were propagated, when appropriate, according to standard methods (39). A P value < 0.05 was considered statistically significant for all assays, excluding genomic analyses where stricter thresholds were applied for large numbers of comparisons (see previously).

Results

TBT pretreatment commits MSCs to the adipose lineage

In a standard MSC adipogenesis assay, cells are seeded and allowed to proliferate until confluency (day 0), and then differentiated for 14 days in the presence of adipogenic cocktail (MDI) and chemicals of interest [Fig. 1(a)] (28). To assess whether TBT can commit MSCs to the adipose lineage, cells were pretreated with chemical ligands for 48 hours (day −2 through day 0), and then induced to differentiate with MDI in the absence of ligands beginning from day 0 [Fig. 1(a)]. Ligand doses were determined using our previous studies in reporter assays, standard MSC adipogenesis assays, and 3T3-L1 adipogenesis assays (18, 21, 22, 28, 40). We ran the standard and commitment assays in parallel, and then assessed lipid accumulation at day 14. Remarkably, MSCs pretreated with TBT or the RXR-selective agonist IRX4204 (4204) (41) for only 48 hours accumulated as much lipid as those exposed for 2 weeks in a standard assay [Fig. 1(b)]. Cells pretreated with the PPARγ agonist ROSI did not accumulate more lipid in the commitment assay than vehicle controls, despite its strong effect in the standard assay [Fig. 1(b)]. Lipids were imaged by fluorescence microscopy to confirm more lipid-containing cells in MSCs pretreated with TBT or 4204 [Fig. 1(c)]. Gene expression analysis conducted at the end of the commitment assay (day 14) confirmed upregulation of adipose lineage markers such as *Fatty acid binding protein 4* (*Fabp4*), *Fat-specific protein 27* (*Fsp27*), and *Lipoprotein lipase* (*Lpl*) in cells pretreated with TBT or 4204, but not ROSI (Supplemental Fig. 1A).

Gene expression was assessed at day 0, following pretreatment but prior to induction of differentiation [Fig. 1(d) and 1(e)]. TBT or 4204 pretreatment upregulated the adipose commitment marker *Zinc finger protein 423* (*Zfp423*), as well as the early differentiation markers *Peroxisome proliferator-activated receptor gamma 2* (*Pparg2*) and *CCAAT/enhancer-binding protein α* (*Cebpa*) [Fig. 1(d)]. Importantly, ROSI pretreatment upregulated the PPARγ target gene *Fabp4*. We infer that PPARγ protein is present, but that its activation is unable to elicit adipogenic commitment in MSCs [Fig. 1(e)]. The RXR target gene, *ATP-binding cassette transporter 1* (*Abca1*), was strongly upregulated by TBT and 4204, but not ROSI [Fig. 1(e)]. Taken together, these data led us to hypothesize that TBT and 4204 commit MSCs to the adipose lineage via a RXR-dependent but PPARγ-independent mechanism.

The adipose and osteogenic lineages are thought to be mutually exclusive (42). Therefore, we conducted the same commitment assay, but instead differentiated pretreated MSCs with an osteogenic cocktail. At day 0, TBT did not alter expression of the osteogenic commitment marker *Runt-related transcription factor 2* (*Runx2*) or the myogenic *Myogenic differentiation 1* (*Myod1*), although there was a slight downregulation of the osteo/chondrogenic marker *SRY-box 9* (*Sox9*) (Supplemental Fig. 1B). Interestingly, pretreatment with ROSI, 4204, or TBT did not inhibit osteogenesis, as assessed by gene expression of bone lineage markers at day 14 (Supplemental Fig. 1C). However, markers of the adipose lineage were persistently upregulated in MSCs pretreated with TBT or 4204 after 2 weeks of osteogenic induction (Supplemental Fig. 1D).

These data suggest that MSCs pretreated with TBT or 4204 are specified (which is reversible), but not determined (which is irreversible), to become adipocytes.

TBT-induced lineage commitment is RXR dependent and PPARγ independent

We used pharmacologic inhibitors of PPARγ and RXR in the commitment assay to test our hypothesis that TBT acts through RXR during lineage commitment. Inhibition of PPARγ with T0070907 during pretreatment did not diminish the effect of TBT or 4204, whereas

the RXR antagonist HX531 attenuated lipid accumulation [Fig. 2(a)]. Expression of *Fabp4* was significantly inhibited by blocking either RXR or PPARγ at day 0, although T0070907 was less effective against TBT or 4204 than against ROSI [Fig. 2(b)]. *Abca1* expression was significantly inhibited by HX531, but unaffected by T0070907 treatment [Fig. 2(b)]. Analysis of early adipogenic marker gene expression revealed RXR-dependent changes in expression, particularly of the key adipogenic gene *Pparg2* [Fig. 2(c)]. These data support a RXR-dependent, PPARγ-independent mechanism of adipose lineage commitment by TBT and RXR activators (rexinoids) such as IRX4204.

To confirm the results of pharmacologic inhibition, we used lentivirus-delivered shRNAs to knock down expression of *Pparg* and *Rxra* in mouse MSCs. Compared with vector-transduced controls, MSCs transduced with lentiviruses expressing shRNAs against *Pparg* and *Rxra* efficiently knocked down their messenger RNA targets at day 0 [Fig. 3(a)]. Although the *Pparg* shRNA was designed to knock down both *Pparg1* and *Pparg2*, *Pparg1* was more efficiently inhibited at day 0 [Fig. 3(a)]. Literature suggests that *Pparg1* is the predominant isoform in undifferentiated MSCs, whereas *Pparg2* expression is induced early in adipogenesis (43). As expected, cells transduced with shRNA targeting *Pparg* or *Rxra* accumulated minimal lipid, irrespective of ligand treatment, because PPARγ and RXR are essential for adipose differentiation [Fig. 3(b)]. At day 0, *Fabp4* expression was greatly diminished by knockdowns of either PPARγ or RXRα. In samples treated with TBT or 4204, *Abca1* expression was slightly reduced in sh*Pparg* MSCs, but strongly inhibited in sh*Rxra* cells [Fig. 3(c)]. Interestingly, knockdown of PPARγ increased basal *Abca1* expression in MSCs treated with DMSO or ROSI, possibly due to increased availability of RXR protein. Expression of the early adipogenic marker genes *Zfp423* and *Cebpa* was diminished by sh*Rxra*, but not sh*Pparg*, suggesting RXR-dependent regulation [Fig. 3(d)]. As seen with *Abca1*, basal expression of these genes increased in

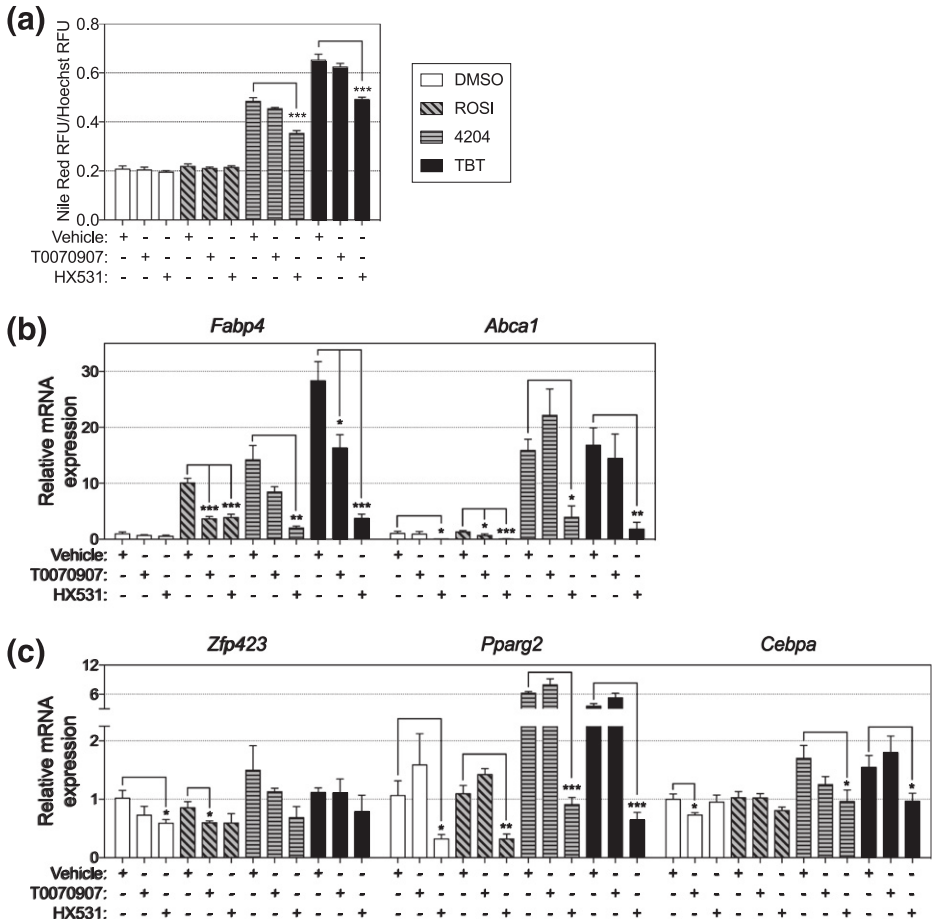

Figure 2. Pharmacologic inhibition of RXR, but not PPARγ, abrogates the effect of TBT pretreatment. MSCs were pretreated for 48 hours with vehicle control (DMSO), ROSI (100 nM), 4204 (100 nM), or TBT (50 nM) in the presence of the PPARγ antagonist T0070907 (100 nM) or the RXR antagonist HX531 (10 uM). (a) Following pretreatment, cells were induced to differentiate with MDI for 14 days and analyzed for lipid accumulation. (b and c) RNA was collected after pretreatment (day 0) for analysis of gene expression by qPCR of (b) canonical PPARγ and RXR targets and (c) early adipose lineage markers. Data are represented as mean ± standard error of the mean. Student *t* test; $*P < 0.05$; $**P < 0.01$; $***P < 0.001$.

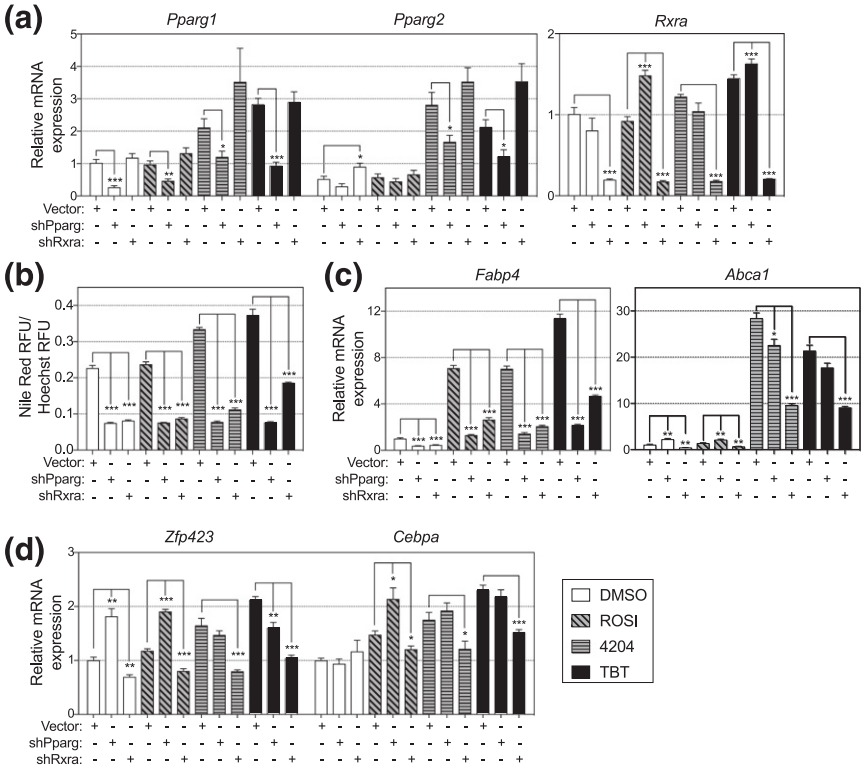

Figure 3. Lentiviral knockdown of RXRα diminishes expression of adipogenic transcriptional targets of TBT and 4204. MSCs were transduced with lentivirus carrying the pLKO.1 vector with and without shRNA against *Pparg* or *Rxra* transcript. Stable lines were treated with vehicle control (DMSO), ROSI (100 nM), 4204 (100 nM), or TBT (50 nM) for 48 hours and then differentiated into adipocytes with an adipogenic induction cocktail (MDI). (a) qPCR of *Pparg* and *Rxra* transcripts at day 0. (b) Lipid accumulation after 2 weeks of adipose induction. (c and d) qPCR analysis of adipogenic gene expression at day 0. Data are represented as mean ± standard error of the mean. Student *t* test; $*P < 0.05$; $**P < 0.01$; $***P < 0.001$.

sh*Pparg* MSCs, suggesting positive regulation by RXR. Taken together, these studies support a RXR-dependent transcriptional regulation of early adipogenic markers by TBT and rexinoids.

RXRs can homodimerize or form heterodimers with several other nuclear receptor partners (44). Therefore, we exposed MSCs to a panel of RXR agonists or agonists of RXR heterodimeric partners to test whether the action of RXR heterodimers or homodimers was required for adipogenic commitment. Pretreatment with TBT, 4204, or another synthetic rexinoid LG100268 increased subsequent adipose differentiation [Fig. 4(a)]. These results were not mirrored by the endogenous RXR activator 9-*cis* retinoic acid [Fig. 4(a)], most likely due to its ability to also activate the retinoic acid receptor (RAR), which inhibits adipogenic differentiation. RAR activators are known to be pro-osteogenic and antiadipogenic (45–47). As expected, pretreatment with all-*trans* retinoic acid or the synthetic RAR agonist arotinoid acid (TTNPB) inhibited adipose differentiation [Fig. 4(a)].

Permissive heterodimers can activate their gene targets in the presence of either a RXR ligand or their own cognate ligands (44). Pretreatment with agonists of the permissive RXR partners PPARα, PPARδ, PPARγ, or liver X receptor (LXR) all failed to commit MSCs to an adipose fate [Fig. 4(b)]. Farnesoid X receptor was not tested because subsequent RNA-seq analysis revealed that it is not expressed in MSCs (data not shown). These data demonstrate that activation of individual permissive heterodimers is insufficient to induce adipose commitment. Treating MSCs with combinations of permissive dimer agonists, however, revealed that targeting PPARδ and PPARγ simultaneously reproduced rexinoid-induced commitment, albeit with less potency [Fig. 4(c)]. Interestingly, the effect of PPARδ/PPARγ agonist combination is attenuated by the further addition of PPARα or LXR agonists [Fig. 4(c)]. Furthermore, simultaneous activation of LXR with PPARα, PPARδ, or a combination of PPARα and PPARγ was mildly adipogenic [Fig. 4(c)]. Taken together, these data show that high-dose activation of several combinations of permissive RXR partners can recapitulate the effect of nanomolar RXR activation. Furthermore, liganded RXR may preferentially act at PPARδ and PPARγ target genes in committing MSCs to the adipose fate.

RNA-Seq analysis confirms the RXR-dependent nature of adipogenic commitment

To better understand what genes might be responsible for adipose lineage commitment, we performed a

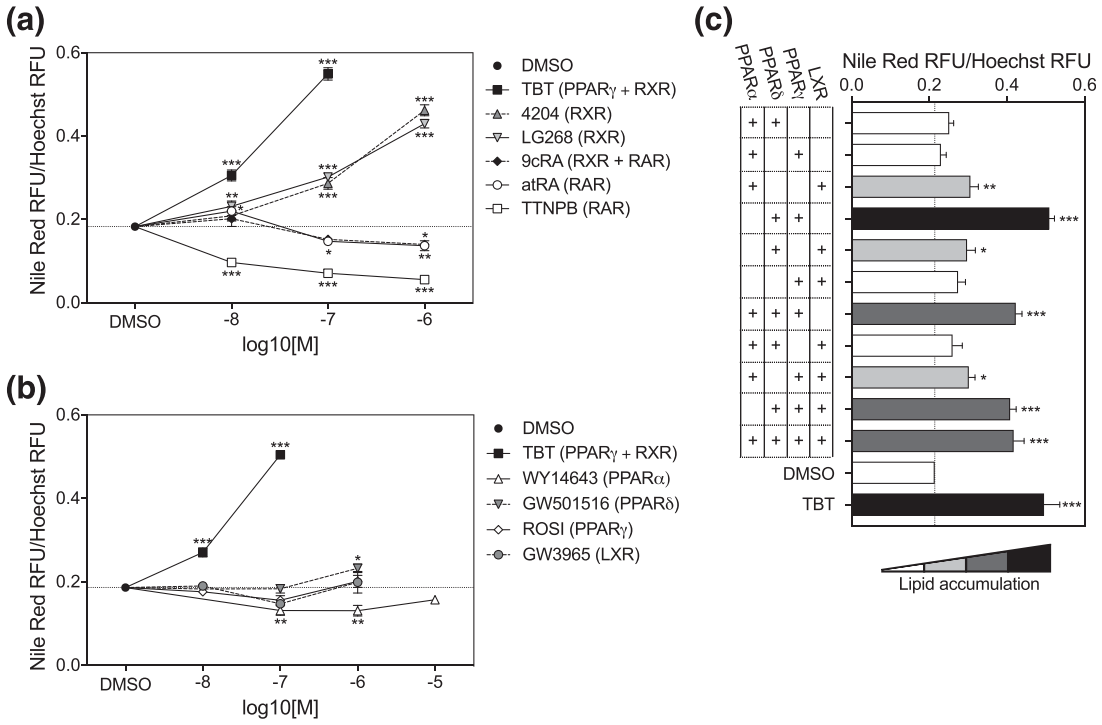

Figure 4. Simultaneous activation of permissive partners of RXR commits MSCs to the adipose fate. MSCs were pretreated for 48 hours with a panel of (a) retinoids and rexinoids or (b and c) agonists of permissive RXR partner receptors, and then differentiated for 2 weeks with MDI. (a) Lipid accumulation was assessed at day 14 following pretreatment with vehicle control (DMSO), TBT, 4204, LG100268, 9-*cis* retinoic acid, all-*trans* retinoic acid, or TTNPB. All treatments were carried out at 10 nM, 100 nM, and 1 μM. (b) Lipid accumulation after 2 weeks of adipose induction following pretreatment with vehicle control (DMSO), TBT, WY14643, GW501516, ROSI, or GW3965. All treatments were carried out at 10 nM, 100 nM, and 1 μM, except for WY14643 (100 nM, 1 μM, and 10 μM) due to its higher half-maximal effective concentration. (c) Lipid accumulation following pretreatment with vehicle control (DMSO), TBT (50 nM), and all possible combinations of WY14643 (10 μM), GW501516 (1 μM), ROSI (1 μM), and GW3965 (1 μM). Data are represented as mean ± standard error of the mean; one-way analysis of variance, Dunnett test; $*P < 0.05$; $**P < 0.01$; $***P < 0.001$.

transcriptomal analysis of MSCs pretreated with TBT (50 nM), 4204 (100 nM), ROSI (100 nM), or vehicle control (0.05% DMSO) (day 0 samples from Fig. 1). Unsupervised hierarchical clustering revealed two distinct clusters: one of TBT and 4204 replicates, and the other of ROSI and DMSO replicates [Fig. 5(a)]. Principal component analysis confirmed these results [Fig. 5(b)]. These data support the existence of a distinct proadipogenic transcriptional program activated by TBT and 4204 via RXR. In contrast, activation of PPARγ by ROSI resulted in minimal overall change in the MSC transcriptome, consistent with the inability of ROSI to elicit adipogenic commitment [Fig. 5(c)]. Analysis of differential gene expression between treatments strengthened these conclusions, showing that TBT and 4204 alter the expression of many of the same transcripts, whereas ROSI altered the expression of few genes [Fig. 5(c); Supplemental Fig. 2A; Supplemental Table 3]. Among the top transcripts upregulated by TBT and 4204 are many well-characterized gene targets of permissive RXR partner receptors, including LXR [*Abca1*, *ATP-binding cassette subfamily G member 1* (*Abcg1*)] and all three PPARs [*Perilipin 4* (*Plin4*), *Fabp4*, *Pyruvate dehydrogenase kinase 4* (*Pdk4*), *Angiopoietin-like 4* (*Angptl4*), *Lipoprotein lipase* (*Lpl*), *Fibroblast growth factor 21* (*Fgf21*)] [Fig. 5(d)]. qPCR confirmed significant changes in gene expression of upregulated and downregulated transcripts (Supplemental Fig. 2B).

Extensive analyses of our transcriptome data were performed by comparing TBT-induced expression changes with previous studies of preadipocyte markers *in vivo* (Supplemental Fig. 3) (13, 48), as well as conducting GO and pathway analyses (Supplemental Fig. 4; Supplemental Table 4). Interestingly, 10 gene sets among the top pathways upregulated by TBT had a corresponding, oppositely-regulated gene set within the top downregulated pathways [red numbers (Supplemental Fig. 4C and 4D). For example, *berenjeno_transformed_by_rhoa_dn* (Supplemental Fig. 4C) and *berenjeno_transformed_by_rhoa_up* (Supplemental Fig. 4D) are gene sets from a study of NIH/3T3 fibroblasts (an uncommitted cell line) transformed with a constitutively active *Ras homolog family member A* (*RhoA*) (49). TBT-induced expression is oppositely correlated with the results in these cells, which is consistent with existing literature showing that RhoA is an antiadipogenic, pro-osteogenic regulator of MSC lineage commitment (50).

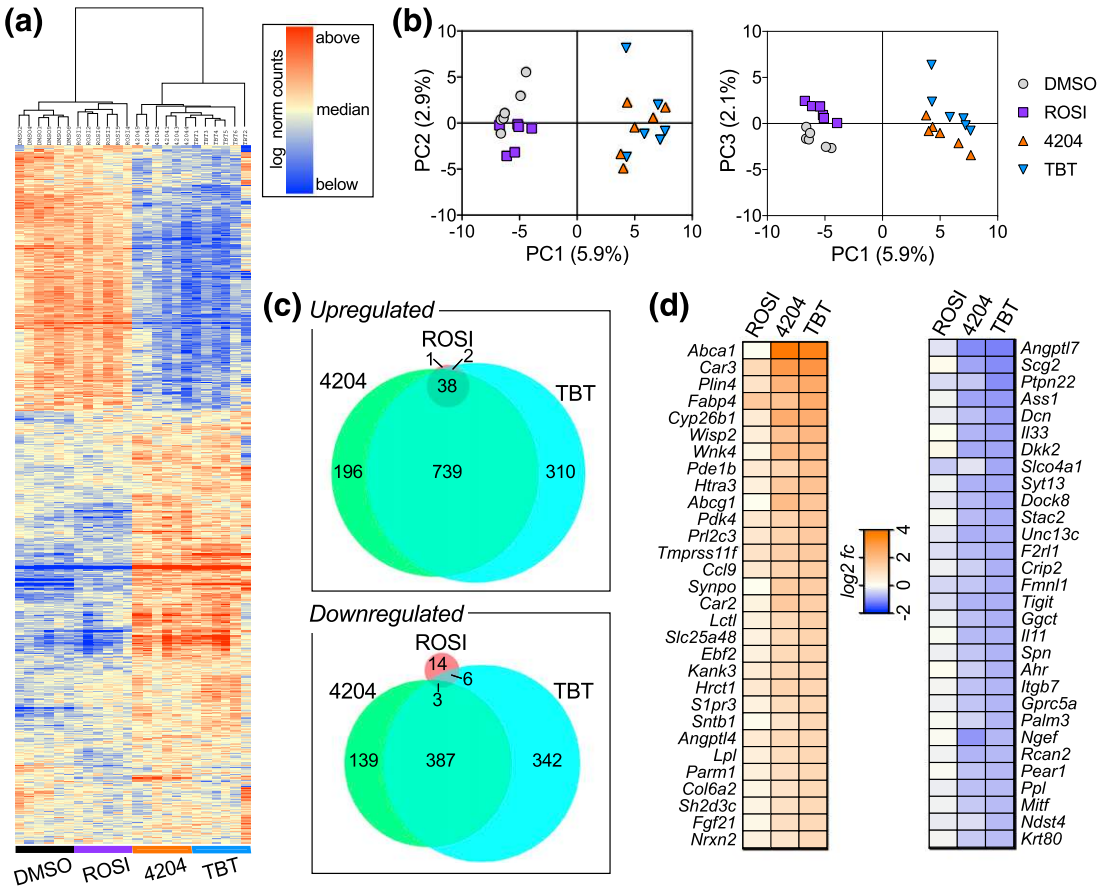

Figure 5. Transcriptomal profiling of MSCs reveals a distinct RXR-dependent transcriptional program in cells treated with 4204 or TBT. RNA from MSCs pretreated for 48 hours with vehicle control (DMSO), ROSI (100 nM), 4204 (100 nM), or TBT (50 nM) was reverse transcribed, subjected to library preparation, and sequenced. Reads were aligned to the mouse genome (STAR aligner), counted (Rsubread), and normalized (DESeq2). (a) Unbiased hierarchical cluster analysis of 908 genes with the highest variance across all treatments and replicates (Cluster 3.0, Java TreeView). (b) Principal component analysis of normalized counts for each treatment and biological replicate was performed (R/Bioconductor). The proportion of the total variance explained by the first three principal components (PCs) is indicated as a percentage. (c) Differential expression relative to vehicle control was analyzed for each chemical treatment (DESeq2); filtered gene lists (Benjamini–Hochberg adjusted P value < 0.01) were queried for overlap of upregulated ($\log_2$ fold change > 0.2) and downregulated ($\log_2$ fold change < -0.2) genes. (d) Ranked list of the top 30 genes upregulated (left) and downregulated (right) by TBT with corresponding expression change for 4204 and ROSI.

RXR activation alters genome-wide H3K27me3 in committing MSCs to the adipose lineage

TBT and 4204-induced changes in gene expression are similar to what was observed with a knockdown of the repressive histone modifier *Enhancer of zeste 2* (*Ezh2*) in PC3 cells (*nuytten_ezh2_targets_up* and *nuytten_ezh2_targets_dn*; Fig S4C-D, number 3) (51). This suggested to us that RXR activation inhibits EZH2 expression, thereby de-repressing critical adipogenic genes. EZH2 is the catalytic member of the Polycomb repressive complex 2 (PRC2), which deposits repressive histone 3 lysine 27 trimethylation (H3K27me3) marks on chromatin. We queried our RNA-Seq data set for all histone-modifying enzymes whose expression was altered by TBT and noted altered expression of several genes known to modify H3K27, including *Ezh1*, *Ezh2*, the H3K27me3 demethylase *Kdm6b* (*Lysine demethylase 6b*), as well as several acetyltransferases (Supplemental Fig. 5A). This led us to hypothesize that TBT acts through RXR to remodel the repressive chromatin landscape and promote adipose lineage commitment. Pretreatment of MSCs with the EZH2 inhibitor DZNep mildly increased subsequent lipid accumulation (Supplemental Fig. 5B). qPCR of MSCs at day 0 revealed that DZNep upregulated important adipogenic genes, including *Ebf1*, *Ebf2*, *Pparg1*, and *Pparg2* (Supplemental Fig. 5C and 5D). The RXR antagonist HX531 inhibited upregulation of proadipogenic transcripts by DZNep, particularly genes that are previously characterized (*Pparg*, *Fabp4*) or suspected (*Ebf2*, *Irx3*) to be direct targets of RXR (Supplemental Fig. 5C–E). Other transcripts upregulated by DZNep were only mildly repressed by HX531 (*Ebf1*, *Foxo1*, *Klf4*), indicating that these may be indirect targets of RXR regulated via EZH2 (Supplemental Fig. 5D and 5E). Notably, *Zfp423* was downregulated by DZNep treatment, suggesting that not all adipogenic targets of RXR are regulated through EZH2 (Supplemental Fig. 5D).

We performed ChIP-Seq analyses of H3K27me3 and H3K4me3 on day 0 MSCs to identify potential genome-wide consequences of RXR activation on chromatin state. Thousands of sharp H3K4me3 peaks were detected, primarily in promoters and gene bodies (Supplemental Fig. 6A–C). Broad H3K27me3 peaks, or islands, were found near genes and at distal intergenic sites in equal proportion (Supplemental Fig. 6A–C). Thousands fewer H3K27me3 islands were detected in TBT-treated MSCs as compared with DMSO (Supplemental Fig. 6A), and TBT reduced the presence of islands near promoters (Supplemental Fig. 6B and 6D). Differential binding analysis of peaks/islands showed a distinct, genome-wide change in H3K27me3 upon RXR activation as assessed by correlation clustering [Fig. 6(b)] and principal component analysis [Fig. 6(c)].

TBT-induced chromatin alterations were more striking for H3K27me3 than H3K4me3 [Fig. 6(a) and 6(b)]. To quantitate the effect of TBT on genome-wide H3K27me3, we assessed the probability density of normalized read counts within differential islands [Fig. 6(d)]. Overall, TBT significantly reduced H3K27me3 within differential islands, primarily due to an enrichment of weak H3K27me3 signal (<5.5 $\log_2$ normalized reads) and confirmed to be significant by Wilcoxon–Mann–Whitney test [Fig. 6(d)]. These data agree with TBT-induced expression changes of *Ezh2* and *Kdm6b* (Supplemental Fig. 5A).

Activation of RXR resulted in thousands of differential islands with altered ChIP signal (Supplemental Fig. 7A; Supplemental Table 5). Given the overall decrease in H3K27me3 upon TBT treatment, we were particularly interested in regions with decreased signal because these sites are susceptible to histone marks that control enhancer activity (52, 53). Distribution of differential islands mirrored genome-wide patterns (Supplemental Figs. 6B and 7B), although decreased islands were overrepresented in distal intergenic regions, suggesting a role at distal enhancers (Supplemental Fig. 7B). Differential H3K27me3 islands were also found within the promoters/gene bodies of DEGs from our RNA-Seq data, many of which have established roles in chromatin modification, cell lineage specification, and adipogenesis (Supplemental Fig. 7C). Because most H3K27me3 islands map to distal sites, we annotated all H3K27me3 differential islands to 4701 neighboring genes (<1 Mb) (Supplemental Fig. 7A). We focused on upregulated DEGs annotated to decreased differential islands and found many regulators of adipogenesis, including *Pparg* and *Cebpa* (Supplemental Fig. 7A). GO term analysis of all genes annotated to decreased

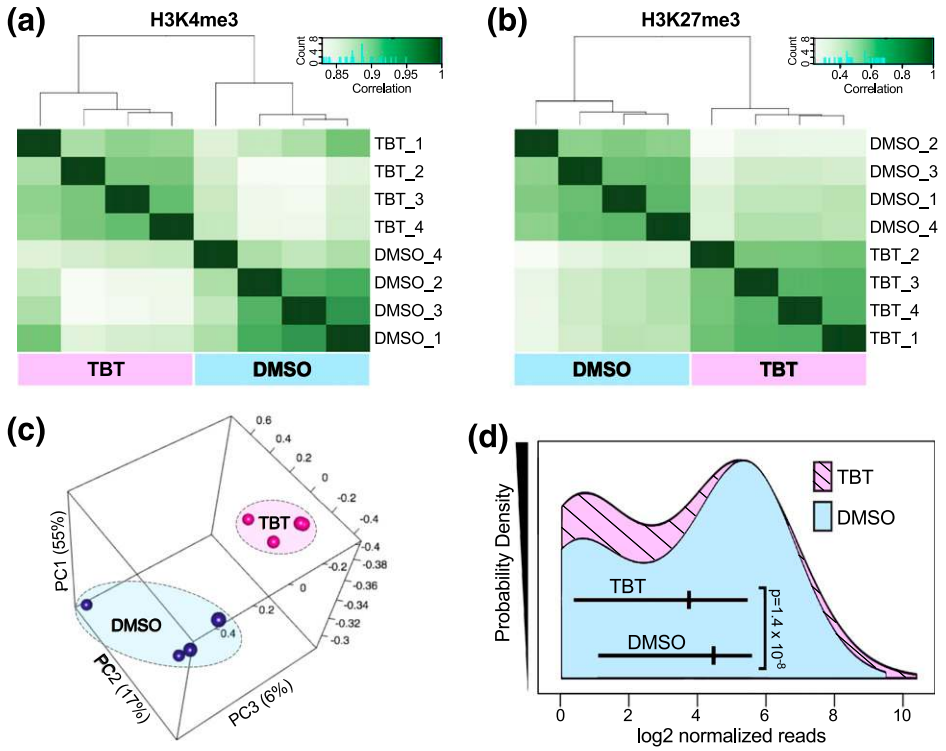

Figure 6. RXR activation in undifferentiated MSCs results in genome-wide alterations of H3K27me3. Chromatin from MSCs pretreated with vehicle control (DMSO) or TBT (50 nM) was immmunoprecipitated for the histone marks H3K4me3 and H3K27me3 and subjected to library preparation and sequencing. Reads were aligned to the mouse genome (mm10), peaks and islands were called in SICER, and differential binding was assessed using DiffBind (R/Bioconductor). (a and b) Correlation clustering of affinity scores within differential islands for (a) H3K4me3 and (b) H3K27me3. (c) Principal component analysis of H3K27me3 affinity scores within differential islands for each sample replicate. (d) Violin plots of normalized reads within H3K27me3 differential islands are shown for DMSO and TBT. *P* value was calculated by two-sided Wilcoxon–Mann–Whitney test.

H3K27me3 islands uncovered several terms concerning development [Fig. 7(a); Supplemental Table 6]. Genes driving these enrichments included known transcriptional regulators of adipogenesis (*Pparg*, *Cebpa*, *Klf4*, *Foxo1*, and *Irx3*), several of which were upregulated DEGs at day 0 [Fig. 7(a)]. Pathway analysis revealed an enrichment of genes from preexisting studies of PRC2 in varied biological systems [Fig. 7(b); Supplemental Table 6]. These gene sets included transcripts that control early adipogenic signals [Fig. 7(b)], many of which were upregulated by the EZH2 inhibitor DZNep (Supplemental Fig. 5E). Taken together, these data indicate that liganded RXR decreases genome-wide H3K27me3 in proximity to genes that regulate adipose commitment.

Discussion

Adipogenesis in humans and mice begins *in utero* and continues during the postnatal period (13–15). Studies in genetic mouse models suggest two distinct adipose progenitor populations *in vivo*: one that develops the fat organ, and another of mural origin that maintains adipose turnover in adults from the perivascular niche (54–56). Both of these progenitors are committed *in utero* (54). Therefore, the prenatal period represents a critical window during which environmental insults can perturb adipose lineage commitment, resulting in potential lasting effects on adiposity in the adult.

TBT is a potent obesogen in rodents exposed prenatally or as adults via activation of the nuclear receptors PPARγ and RXR (18, 21, 57, 58). The obesogenic effects of prenatal TBT exposure are propagated transgenerationally to unexposed generations, presumably via epigenetic modifications of the germline (20, 59). Undifferentiated MSCs from mice prenatally exposed to TBT have a proadipogenic, antiosteogenic gene expression profile (20, 21), which led us to

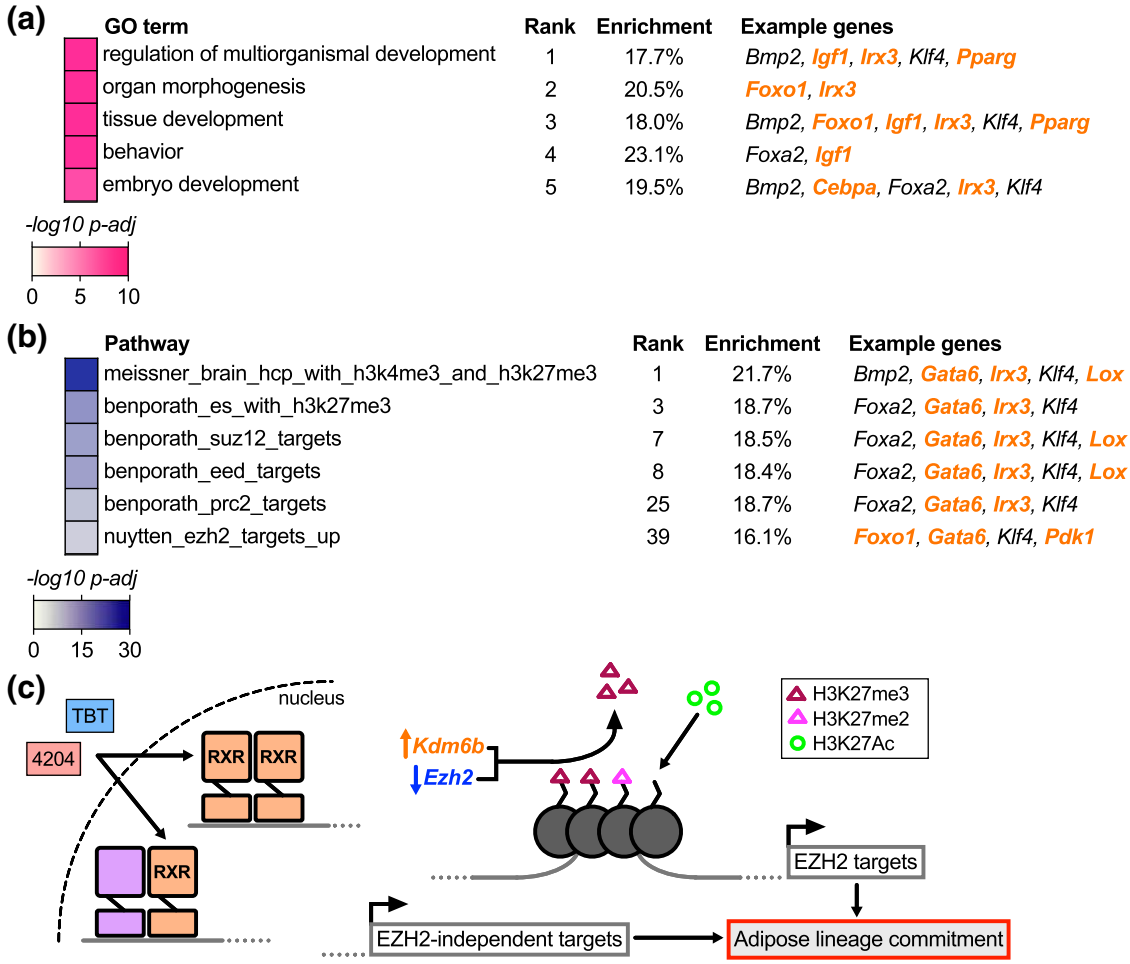

Figure 7. TBT alters H3K27me3 near-transcriptional regulators that control adipogenesis. H3K27me3 differential islands were annotated to neighboring genes (<1 Mb) using Genomic Regions Enrichment of Annotations Tool. (a and b) Differential islands decreased by TBT treatment were annotated to 2803 genes. These genes were subjected to (a) GO term and (b) pathway analysis and ranked by Benjamini–Hochberg adjusted *P* values. The fraction of annotated genes found in each GO term or pathway is displayed as a percentage. Examples of annotated genes are shown; genes that are upregulated DEGs in our RNA-seq data set are shown in bold type. (b) Pathways enriched in genes proximal to differential islands decreased upon TBT treatment that are from previous studies of the PRC2 complex. (c) Model of RXR-induced adipose lineage commitment of MSCs.

investigate how TBT influences early cell fate decisions in MSCs.

Current understanding of adipose lineage commitment lags behind that of terminal differentiation (60). This is in part due to the popularity of the 3T3-L1 cell line (which is a committed preadipocyte line) and an emphasis on the master regulator PPARγ, despite that induction of PPARγ2 expression occurs after lineage commitment (16, 60). *In vitro* models of commitment have been limited because the components of adipose induction cocktails induce both commitment and differentiation of MSCs, making it difficult to decipher when each phase begins and ends. To circumvent these issues, we developed a commitment assay using primary bone marrow–derived MSCs and used it to show that a 2-day pretreatment with TBT or the rexinoid IRX4204 was as potent inducing adipogenesis as a 14-day cotreatment with induction cocktail (the standard assay) (Fig. 1). We went on to show that adipogenic commitment is RXR dependent (Figs. 2 and 3), revealing that RXR activation is sufficient for the adipogenic commitment of MSCs. Furthermore, we show that TBT reduces and redistributes genome-wide H3K27me3 in programming adipose lineage bias (Figs. 6 and 7). Hence, we have provided an *in vitro* model of an environmental exposure altering the epigenome of a stem cell compartment to perturb subsequent development. Studying this phenomenon mechanistically *in vitro* may shed light on how *in utero* exposures can program disease risk in adulthood (6).

RXR is a unique member of the nuclear receptor superfamily because it heterodimerizes with many other receptors (44). We therefore investigated whether TBT acts as a homodimer or in concert with permissive RXR heterodimers in committing MSCs to an adipose fate. Chemical inhibition of PPARγ in MSCs only partially blocks induction of its canonical target gene, *Fabp4*, by rexinoids [Fig. 2(b)]. We previously showed, however, that the PPARγ/RXR heterodimer remains permissive in the presence of a PPARγ antagonist (22). Lentiviral knockdown of PPARγ ablates induction of *Fabp4* by RXR agonists [Fig. 3(c)], suggesting that liganded RXR must act as a PPARγ/RXR heterodimer at *Fabp4* and likely other loci. Interestingly, *Pparg* knockdown slightly attenuated rexinoid-induced upregulation of *Abca1* and *Zfp423* [Fig. 3(c) and 3(d)]. Thus, whereas these transcripts are predominantly regulated by other permissive partners or RXR homodimers, they obtain some activation from PPARγ/RXR heterodimers in the presence of RXR activators. We also noted several discrepancies between chemical inhibition of RXR with HX531 (Fig. 2) and lentiviral knockdown of RXRα (Fig. 3). For example, HX531 strongly inhibited *Pparg2*, but not *Zfp423* expression [Fig. 2(c)]; the opposite trends were observed in lentiviral knockdown of RXRα [Fig. 3(a) and 3(d)]. These differences may be due to compensation by RXRβ when RXRα is knocked down (RXRγ is not expressed in MSCs), or to RXR-mediated recruitment of corepressors that can take place during chemical inhibition, but not when the receptor is knocked down.

Pretreatment of MSCs with individual permissive heterodimer agonists failed to commit MSCs to an adipose fate [Fig. 4(b)]. However, combining PPARδ and PPARγ agonists at micromolar doses successfully reproduced the effect of nanomolar rexinoid pretreatment, more effectively than other combinations of PPAR and LXR agonists [Fig. 4(c)]. In 3T3-L1 cells, permissive PPARδ/RXR heterodimers occupy key adipogenic sites early in differentiation, days before PPARγ/RXR is detected (61). Hence, RXR may preferentially bind PPARδ and PPARγ gene targets in committing MSCs to the adipose fate. The ability of RXR to recruit and target multiple partners from the nuclear receptor pool likely contributes to the unique ability of rexinoids to alter MSC fate.

Transcriptomal profiling of MSCs exposed to TBT identified a distinct RXR-dependent transcriptional program (Fig. 5; Supplemental Fig. 2A; Supplemental Table 3). GO analysis of transcripts upregulated by TBT revealed genes enriched for terms associated with extracellular matrix (ECM) proteins, which are known to play a role in MSC commitment (16), and lipid metabolism genes, which include many well-known regulators of adipogenesis and adipocyte function [*Pparg*, *Cebpa*, *Sterol regulatory element-binding protein 1* (*Srebf1*), *Cluster of differentiation 36* (*Cd36*), *Lipase E* (*Lipe*, also known as hormone-sensitive lipase)] (Supplemental Fig 4A; Supplemental Table 4). Transcripts downregulated by TBT and 4204 were enriched for cell cycle–related terms, indicating that these cells are exiting the cell cycle as they become committed preadipocytes (Supplemental Fig. 4B; Supplemental Table 4).

We compared TBT-induced expression changes with previously published datasets characterizing the transcriptome of committed preadipocytes *in vivo* (Supplemental Fig. 3). Graff *et al.* (13) used genetic reporter mice to show that adipose expansion in the early postnatal period arises from PPARγ-expressing progenitors that are committed prenatally and reside, in part, within the perivascular niche. Not surprisingly, PPARγ$^+$ stromal vascular fraction and TBT or rexinoid-treated MSCs both show upregulation of PPARγ target genes, such as *Angptl4*, *Nr1h3* (LXRα), *Cebpa*, and *Pyruvate carboxylase* (*Pcx*) (Supplemental Fig. 3C). This suggests that the ability of liganded RXR to activate PPARγ target genes is central to RXR-induced adipose commitment of MSCs.

Spiegelman *et al.* (62) identified *Zfp423* as a regulator of adipose commitment upstream of PPARγ, and subsequently used reporter mice to show that *Zfp423* marks committed preadipocytes *in vivo*, also within the perivascular niche (48). Two of the most enriched genes in Zfp423$^+$ stromal vascular fraction are *Ebf1* and *Ebf2*, both of which are upregulated by TBT and 4204 (Supplemental Fig. 3B). *Ebf1* or *Ebf2* overexpression in uncommitted NIH 3T3 fibroblasts promotes adipogenesis upstream of PPARγ, whereas knockdown of either gene inhibits adipogenesis (63). Therefore, we infer that *Ebf1* and *Ebf2* are critical regulators of RXR-induced lineage commitment of MSCs, acting upstream of PPARγ. Genes significantly upregulated in both *in vivo* studies and our TBT-treated MSCs included the master regulator of adipose differentiation *Pparg* and the pericyte/preadipocyte marker *Platelet-derived growth factor receptor β* (*Pdgfrb*) (Supplemental Fig. 3A) (64). Downregulated transcripts included two of the top five genes repressed by TBT, *Angiopoietin-like 7* (*Angptl7*) and *Argininosuccinate synthase 1* (*Ass1*) (Supplemental Fig. 3A), whose functions in adipogenesis are unknown. Taken together, these data show that RXR activation induces gene expression changes in MSCs that define the preadipocyte *in vivo*.

Previous work in bone marrow–derived macrophages showed that RXR ligands do not alter the genomic distribution of RXR, but rather increase recruitment of transcriptional activators and histone modifiers to preestablished RXR binding sites (65). Our pathway analysis of TBT-regulated genes suggested a RXR-dependent inhibition of the repressive histone modifier EZH2 (Supplemental Fig. 4C and 4D). Chemical inhibition of EZH2 increased expression of several adipogenic regulators, such as *Ebf1*, *Ebf2*, *Pparg1*, and *Pparg2*, but not others, such as *Zfp423* and *Cebpa* (Supplemental Fig. 5C and 5D). These conflicting changes in gene expression may explain the mild overall effect of DZNep on lipid accumulation (Supplemental Fig. 5B) and suggests that not all adipogenic targets of RXR are regulated through EZH2. Notably, RXR activation also diminishes expression of the H3K9me3 methyltransferase *Suppression of variegation 3-9 homolog 2* (*Suv39h2*). H3K9me3 has previously been shown to regulate expression of *Pparg* and *Cebpa* at their promoters in 3T3-L1 cells (66).

EZH2 was previously implicated as a positive regulator of adipogenesis and an inhibitor of osteogenesis through regulation of H3K27me3 at the promoters of WNT genes (67–70). In contrast to our work, these studies were carried out either in preadipocytes or in MSCs following treatment with adipogenic or osteogenic induction cocktails and did not assess the genome-wide chromatin state in undifferentiated MSCs, where EZH2 appears to have a distinct role in lineage allocation. Our analysis of H3K27me3 revealed a striking, RXR-induced redistribution and reduction of this repressive mark [Fig. 6(b–d); Supplemental Fig. 6D; Supplemental Table 5]. Pathway analysis of genes in proximity to decreased H3K27me3 islands revealed an enrichment of gene sets from previous studies of PRC2, suggesting that liganded RXR alters H3K27me3 near bona fide targets of PRC2 [Fig. 7(b)]. These genes included *Insulin growth factor 1* (*Igf1*), *Iriquois homeobox 3* (*Irx3*), *Kruppel-like factor 4* (*Klf4*), and *Lysyl oxidase* (*Lox*), all of which have been implicated as positive regulators of early adipogenesis (24, 71–73). Importantly, both *Irx3* and *Klf4* were upregulated by the EZH2 inhibitor DZNep (Supplemental Fig. 5E). Future studies will attempt to decipher which genes are direct targets of RXR and which are regulated through EZH2. In addition, we aim to confirm RXR-dependent changes in H3K27me3 near critical adipogenic regulators (*Pparg*, *Ebf1*, *Ebf2*, *Irx3*, *Klf4*) by ChIP-Seq in the presence and absence of 4204 and HX531.

In human and mouse embryonic stem (ES) cells, H3K27me3 marks poised distal enhancers and has a well-studied reciprocal relationship with H3K27Ac, a mark of active enhancers (53). A recent study of chromatin dynamics during osteogenic differentiation confirmed the presence of these marks at distal enhancers in mouse bone marrow–derived MSCs and described their importance during osteogenesis (74). Furthermore, the EZH2-mediated divalent H3K27me2 mark has now been implicated in distal enhancer regulation and lineage specification of ES cells (52, 75). Hence, RXR-regulated demethylation of H3K27 may leave differential sites susceptible to modifications that interfere with enhancer activity in undifferentiated MSCs. In macrophages, RXR is known to influence gene expression through long-range enhancers (65). Therefore, RXR-initiated genome-wide changes in H3K27me3 may reflect a broader restructuring of the nuclear architecture that influences subsequent development (76). Further studies into how EDCs can reorganize the chromatin of stem cell compartments should provide critical evidence in understanding how developmental exposures program disease risk later in life and propagate that risk to future generations.

Conservative estimates of the cost of endocrine disruption in the United States and Europe are in the hundreds of billions of dollars annually, with a significant portion attributed to increases in obesity and diabetes (77–79). Many xenobiotic chemicals are known to promote adipogenesis through nuclear receptors such as PPARγ and estrogen receptor (8, 9). Few chemicals other than TBT have been definitively identified as RXR

Appendix. Antibody Table

Peptide/Protein Target	Antigen Sequence (if Known)	Name of Antibody	Manufacturer, Catalog No.	Species Raised in; Monoclonal or Polyclonal	Dilution Used	RRID
Histone 3 lysine 4 trimethyl	Proprietary	Anti-H3K4me3	Abcam, ab8580	Rabbit; polyclonal	2.5 μg/5 μg DNA (ChIP)	AB_306649
Histone 3 lysine 27 trimethyl	Proprietary	Anti-H3K27me3	Abcam, ab6002	Mouse; monoclonal	2.5 μg/5 μg DNA (ChIP)	AB_305237

Abbreviation: RRID, research resource identifier.

activators, with the fungicide fludioxonil (40) and the nonionic surfactant Span 80 (80) being two notable exceptions. Considering that our data reveal a role for RXR in MSC lineage specification, a concerted effort to determine whether there are other, bona fide chemical activators of RXR that can act as obesogens may be worthwhile. The ability of rexinoids or dual RXR–PPARγ activators such as TBT, but not strong PPARγ activators such as ROSI, to elicit transgenerational effects on fat accumulation (20) underscores the potential importance of this effort. Within the EDC field, 3T3-L1 cells remain the most popular tool for screening and characterizing obesogens *in vitro*, despite their inability to model lineage commitment and long-standing issues with reproducibility across laboratories and vendors (81–84). Our commitment assay offers an approach to identify chemicals that can affect lineage specification upstream of PPARγ in a primary, multipotent stem cell model. Moreover, this approach offered insights into the biology of MSC lineage commitment that would not have been apparent in a standard MSC assay.

RXR is known for its roles in adipogenic (27) and myogenic (85) terminal differentiation, in myogenic commitment of ES cells (86), and for its dramatic effects on the epigenome of macrophages (65). Here we report a role for RXR in the lineage commitment of MSCs and show that RXR activation in MSCs produces genome-wide reduction and redistribution of H3K27me3 marks to promote adipose lineage commitment. These data identify RXR as an important interface between the environment and the epigenome that can influence the developmental programming of obesity. RXR is widely expressed *in utero* and has multiple roles in the development of tissues such as the eye, brain, heart, and, importantly, the placenta and gametes (87, 88). This raises concerns that RXR activators may disrupt the development of multiple organ systems, and raises the stakes for effectively identifying which chemicals in production can activate RXR *in vitro* and *in vivo*. In particular, the investigation of developmental RXR disruption in the placenta, gametes, and the soma that support gametogenesis may prove critical in understanding how EDCs such as TBT can propagate disease risk over multiple generations.

Acknowledgments

We thank all members of the Blumberg and Shioda laboratories. In particular, we thank Dr. Raquel Chamorro-García and Dr. Amanda Janesick for intellectual contributions to the project, and Keiko Shioda for work preparing lentivirus and libraries for sequencing. We thank Rosh Chandraratna, IO Therapeutics (Santa Ana, CA), for a gift of IRX4204.

Financial Support: This work was supported by Grant R01ES023316 from the National Institute of Environmental Health Sciences (to B.B. and T.S.), Grant 15PRE25090030 from the American Heart Association (to B.M.S.), and Grant STAR FP917800 from the Environmental Protection Agency (to B.M.S.).

Author Contributions: B.M.S., T.S., and B.B. designed the experiments, wrote the manuscript, and secured funding. B.M.S., E.S.M., T.J.A., V.T.H., and Z.M. performed all experiments. B.M.S. and T.S. analyzed the data.

Correspondence and Reprint Requests: Bruce Blumberg, PhD, University of California, Irvine, 2011 Biological Sciences 3, Irvine, California 92697-2300. E-mail: blumberg@uci.edu; or Toshi Shioda, MD, PhD, Massachusetts General Hospital Center for Cancer Research, Building 149 - 7th floor, 13th Street, Charlestown, Massachusetts 02129. E-mail: tshioda@partners.org.

Disclosure Summary: B.B. is a named inventor on several patents related to PPARγ. The remaining authors have nothing to disclose.

References

1. Flegal KM, Kruszon-Moran D, Carroll MD, Fryar CD, Ogden CL. Trends in obesity among adults in the United States, 2005 to 2014. *JAMA*. 2016;**315**(21):2284–2291.
2. Ogden CL, Carroll MD, Lawman HG, Fryar CD, Kruszon-Moran D, Kit BK, Flegal KM. Trends in obesity prevalence among children and adolescents in the United States, 1988-1994 through 2013-2014. *JAMA*. 2016;**315**(21):2292–2299.
3. Cawley J, Meyerhoefer C. The medical care costs of obesity: an instrumental variables approach. *J Health Econ*. 2012;**31**(1):219–230.
4. Hall KD, Heymsfield SB, Kemnitz JW, Klein S, Schoeller DA, Speakman JR. Energy balance and its components: implications for body weight regulation. *Am J Clin Nutr*. 2012;**95**(4):989–994.
5. National Institutes of Health. Clinical guidelines on the identification, evaluation, and treatment of overweight and obesity in adults–the evidence report. *Obes Res*. 1998;**6**(Suppl 2):51S–209S.

6. Hanson MA, Gluckman PD. Early developmental conditioning of later health and disease: physiology or pathophysiology? *Physiol Rev*. 2014;**94**(4):1027–1076.
7. Janesick AS, Blumberg B. Obesogens: an emerging threat to public health. *Am J Obstet Gynecol*. 2016;**214**(5):559–565.
8. Heindel JJ, Skalla LA, Joubert BR, Dilworth CH, Gray KA. Review of developmental origins of health and disease publications in environmental epidemiology. *Reprod Toxicol*. 2017;**68**:34–48.
9. Heindel JJ, Blumberg B, Cave M, Machtinger R, Mantovani A, Mendez MA, Nadal A, Palanza P, Panzica G, Sarqis R, Vandenberg LN, Vom Saal F. Metabolism disrupting chemicals and metabolic disorders. *Reprod Toxicol*. 2017;**68**:3–33.
10. Grün F, Blumberg B. Environmental obesogens: organotins and endocrine disruption via nuclear receptor signaling. *Endocrinology*. 2006;**147**(6, Suppl):S50–S55.
11. Gore AC, Chappell VA, Fenton SE, Flaws JA, Nadal A, Prins GS, Toppari J, Zoeller RT. EDC-2: the Endocrine Society's second scientific statement on endocrine-disrupting chemicals. *Endocr Rev*. 2015;**36**(6):E1–E150.
12. Janesick A, Blumberg B. Endocrine disrupting chemicals and the developmental programming of adipogenesis and obesity. *Birth Defects Res C Embryo Today*. 2011;**93**(1):34–50.
13. Tang W, Zeve D, Suh JM, Bosnakovski D, Kyba M, Hammer RE, Tallquist MD, Graff JM. White fat progenitor cells reside in the adipose vasculature. *Science*. 2008;**322**(5901):583–586.
14. Poissonnet CM, Burdi AR, Bookstein FL. Growth and development of human adipose tissue during early gestation. *Early Hum Dev*. 1983;**8**(1):1–11.
15. Wang QA, Tao C, Gupta RK, Scherer PE. Tracking adipogenesis during white adipose tissue development, expansion and regeneration. *Nat Med*. 2013;**19**(10):1338–1344.
16. Cristancho AG, Lazar MA. Forming functional fat: a growing understanding of adipocyte differentiation. *Nat Rev Mol Cell Biol*. 2011;**12**(11):722–734.
17. Tontonoz P, Spiegelman BM. Fat and beyond: the diverse biology of PPARgamma. *Annu Rev Biochem*. 2008;**77**:289–312.
18. Grün F, Watanabe H, Zamanian Z, Maeda L, Arima K, Cubacha R, Gardiner DM, Kanno J, Iguchi T, Blumberg B. Endocrine-disrupting organotin compounds are potent inducers of adipogenesis in vertebrates. *Mol Endocrinol*. 2006;**20**(9):2141–2155.
19. Kanayama T, Kobayashi N, Mamiya S, Nakanishi T, Nishikawa J. Organotin compounds promote adipocyte differentiation as agonists of the peroxisome proliferator-activated receptor gamma/retinoid X receptor pathway. *Mol Pharmacol*. 2005;**67**(3):766–774.
20. Chamorro-García R, Sahu M, Abbey RJ, Laude J, Pham N, Blumberg B. Transgenerational inheritance of increased fat depot size, stem cell reprogramming, and hepatic steatosis elicited by prenatal exposure to the obesogen tributyltin in mice. *Environ Health Perspect*. 2013;**121**(3):359–366.
21. Kirchner S, Kieu T, Chow C, Casey S, Blumberg B. Prenatal exposure to the environmental obesogen tributyltin predisposes multipotent stem cells to become adipocytes. *Mol Endocrinol*. 2010;**24**(3):526–539.
22. Li X, Ycaza J, Blumberg B. The environmental obesogen tributyltin chloride acts via peroxisome proliferator activated receptor gamma to induce adipogenesis in murine 3T3-L1 preadipocytes. *J Steroid Biochem Mol Biol*. 2011;**127**(1-2):9–15.
23. Tang QQ, Otto TC, Lane MD. Commitment of C3H10T1/2 pluripotent stem cells to the adipocyte lineage. *Proc Natl Acad Sci USA*. 2004;**101**(26):9607–9611.
24. Huang H, Song TJ, Li X, Hu L, He Q, Liu M, Lane MD, Tang QQ. BMP signaling pathway is required for commitment of C3H10T1/2 pluripotent stem cells to the adipocyte lineage. *Proc Natl Acad Sci USA*. 2009;**106**(31):12670–12675.
25. Bowers RR, Kim JW, Otto TC, Lane MD. Stable stem cell commitment to the adipocyte lineage by inhibition of DNA methylation: role of the BMP-4 gene. *Proc Natl Acad Sci USA*. 2006;**103**(35):13022–13027.
26. Imai T, Jiang M, Chambon P, Metzger D. Impaired adipogenesis and lipolysis in the mouse upon selective ablation of the retinoid X receptor alpha mediated by a tamoxifen-inducible chimeric Cre recombinase (Cre-ERT2) in adipocytes. *Proc Natl Acad Sci USA*. 2001;**98**(1):224–228.
27. Tontonoz P, Singer S, Forman BM, Sarraf P, Fletcher JA, Fletcher CD, Brun RP, Mueller E, Altiok S, Oppenheim H, Evans RM, Spiegelman BM. Terminal differentiation of human liposarcoma cells induced by ligands for peroxisome proliferator-activated receptor gamma and the retinoid X receptor. *Proc Natl Acad Sci USA*. 1997;**94**(1):237–241.
28. Chamorro-García R, Kirchner S, Li X, Janesick A, Casey SC, Chow C, Blumberg B. Bisphenol A diglycidyl ether induces adipogenic differentiation of multipotent stromal stem cells through a peroxisome proliferator-activated receptor gamma-independent mechanism. *Environ Health Perspect*. 2012;**120**(7):984–989.
29. Livak KJ, Schmittgen TD. Analysis of relative gene expression data using real-time quantitative PCR and the 2(-Delta Delta C(T)) method. *Methods*. 2001;**25**(4):402–408.
30. Lee TI, Johnstone SE, Young RA. Chromatin immunoprecipitation and microarray-based analysis of protein location. *Nat Protoc*. 2006;**1**(2):729–748.
31. Dobin A, Davis CA, Schlesinger F, Drenkow J, Zaleski C, Jha S, Batut P, Chaisson M, Gingeras TR. STAR: ultrafast universal RNA-seq aligner. *Bioinformatics*. 2013;**29**(1):15–21.
32. Li H, Handsaker B, Wysoker A, Fennell T, Ruan J, Homer N, Marth G, Abecasis G, Durbin R; 1000 Genome Project Data Processing Subgroup. The sequence alignment/map format and SAMtools. *Bioinformatics*. 2009;**25**(16):2078–2079.
33. Liao Y, Smyth GK, Shi W. The Subread aligner: fast, accurate and scalable read mapping by seed-and-vote. *Nucleic Acids Res*. 2013;**41**(10):e108.
34. Love MI, Huber W, Anders S. Moderated estimation of fold change and dispersion for RNA-seq data with DESeq2. *Genome Biol*. 2014;**15**(12):550.
35. Xu S, Grullon S, Ge K, Peng W. Spatial clustering for identification of ChIP-enriched regions (SICER) to map regions of histone methylation patterns in embryonic stem cells. *Methods Mol Biol*. 2014;**1150**:97–111.
36. Ross-Innes CS, Stark R, Teschendorff AE, Holmes KA, Ali HR, Dunning MJ, Brown GD, Gojis O, Ellis IO, Green AR, Ali S, Chin SF, Palmieri C, Caldas C, Carroll JS. Differential oestrogen receptor binding is associated with clinical outcome in breast cancer. *Nature*. 2012;**481**(7381):389–393.
37. Yu G, Wang LG, He QY. ChIPseeker: an R/Bioconductor package for ChIP peak annotation, comparison and visualization. *Bioinformatics*. 2015;**31**(14):2382–2383.
38. McLean CY, Bristor D, Hiller M, Clarke SL, Schaar BT, Lowe CB, Wenger AM, Bejerano G. GREAT improves functional interpretation of cis-regulatory regions. *Nat Biotechnol*. 2010;**28**(5):495–501.
39. Bevington PR, Robinson DK. *Data Reduction and Error Analysis for the Physical Sciences*. 3rd ed. Boston, MA: McGraw-Hill; 2003.
40. Janesick AS, Dimastrogiovanni G, Vanek L, Boulos C, Chamorro-García R, Tang W, Blumberg B. On the utility of ToxCast™ and ToxPi as methods for identifying new obesogens. *Environ Health Perspect*. 2016;**124**(8):1214–1226.
41. Vuligonda V, Thacher SM, Chandraratna RA. Enantioselective syntheses of potent retinoid X receptor ligands: differential biological activities of individual antipodes. *J Med Chem*. 2001;**44**(14):2298–2303.
42. Kang Q, Song WX, Luo Q, Tang N, Luo J, Luo X, Chen J, Bi Y, He BC, Park JK, Jiang W, Tang Y, Huang J, Su Y, Zhu GH, He Y, Yin H, Hu Z, Wang Y, Chen L, Zuo GW, Pan X, Shen J, Vokes T, Reid RR, Haydon RC, Luu HH, He TC. A comprehensive analysis of the dual roles of BMPs in regulating adipogenic and osteogenic

differentiation of mesenchymal progenitor cells. *Stem Cells Dev*. 2009;**18**(4):545–559.
43. Aprile M, Ambrosio MR, D'Esposito V, Beguinot F, Formisano P, Costa V, Ciccodicola A. PPARG in human adipogenesis: differential contribution of canonical transcripts and dominant negative isoforms. *PPAR Res*. 2014;**2014**:537865.
44. Evans RM, Mangelsdorf DJ. Nuclear receptors, RXR, and the Big Bang. *Cell*. 2014;**157**(1):255–266.
45. Lee JS, Park JH, Kwon IK, Lim JY. Retinoic acid inhibits BMP4-induced C3H10T1/2 stem cell commitment to adipocyte via downregulating Smad/p38MAPK signaling. *Biochem Biophys Res Commun*. 2011;**409**(3):550–555.
46. Marchildon F, St-Louis C, Akter R, Roodman V, Wiper-Bergeron NL. Transcription factor Smad3 is required for the inhibition of adipogenesis by retinoic acid. *J Biol Chem*. 2010;**285**(17): 13274–13284.
47. Schwarz EJ, Reginato MJ, Shao D, Krakow SL, Lazar MA. Retinoic acid blocks adipogenesis by inhibiting C/EBPbeta-mediated transcription. *Mol Cell Biol*. 1997;**17**(3):1552–1561.
48. Gupta RK, Mepani RJ, Kleiner S, Lo JC, Khandekar MJ, Cohen P, Frontini A, Bhowmick DC, Ye L, Cinti S, Spiegelman BM. Zfp423 expression identifies committed preadipocytes and localizes to adipose endothelial and perivascular cells. *Cell Metab*. 2012;**15**(2):230–239.
49. Berenjeno IM, Núñez F, Bustelo XR. Transcriptomal profiling of the cellular transformation induced by Rho subfamily GTPases. *Oncogene*. 2007;**26**(29):4295–4305.
50. McBeath R, Pirone DM, Nelson CM, Bhadriraju K, Chen CS. Cell shape, cytoskeletal tension, and RhoA regulate stem cell lineage commitment. *Dev Cell*. 2004;**6**(4):483–495.
51. Nuytten M, Beke L, Van Eynde A, Ceulemans H, Beullens M, Van Hummelen P, Fuks F, Bollen M. The transcriptional repressor NIPP1 is an essential player in EZH2-mediated gene silencing. *Oncogene*. 2008;**27**(10):1449–1460.
52. Ferrari KJ, Scelfo A, Jammula S, Cuomo A, Barozzi I, Stützer A, Fischle W, Bonaldi T, Pasini D. Polycomb-dependent H3K27me1 and H3K27me2 regulate active transcription and enhancer fidelity. *Mol Cell*. 2014;**53**(1):49–62.
53. Calo E, Wysocka J. Modification of enhancer chromatin: what, how, and why? *Mol Cell*. 2013;**49**(5):825–837.
54. Jiang Y, Berry DC, Tang W, Graff JM. Independent stem cell lineages regulate adipose organogenesis and adipose homeostasis. *Cell Reports*. 2014;**9**(3):1007–1022.
55. Hong KY, Bae H, Park I, Park DY, Kim KH, Kubota Y, Cho ES, Kim H, Adams RH, Yoo OJ, Koh GY. Perilipin+ embryonic preadipocytes actively proliferate along growing vasculatures for adipose expansion. *Development*. 2015;**142**(15):2623–2632.
56. Wang QA, Tao C, Jiang L, Shao M, Ye R, Zhu Y, Gordillo R, Ali A, Lian Y, Holland WL, Gupta RK, Scherer PE. Distinct regulatory mechanisms governing embryonic versus adult adipocyte maturation. *Nat Cell Biol*. 2015;**17**(9):1099–1111.
57. Bertuloso BD, Podratz PL, Merlo E, de Araújo JF, Lima LC, de Miguel EC, de Souza LN, Gava AL, de Oliveira M, Miranda-Alves L, Carneiro MT, Nogueira CR, Graceli JB. Tributyltin chloride leads to adiposity and impairs metabolic functions in the rat liver and pancreas. *Toxicol Lett*. 2015;**235**(1):45–59.
58. Zuo Z, Chen S, Wu T, Zhang J, Su Y, Chen Y, Wang C. Tributyltin causes obesity and hepatic steatosis in male mice. *Environ Toxicol*. 2011;**26**(1):79–85.
59. Chamorro-García R, Blumberg B. Transgenerational effects of obesogens and the obesity epidemic. *Curr Opin Pharmacol*. 2014; **19**:153–158.
60. Rosen ED, Spiegelman BM. What we talk about when we talk about fat. *Cell*. 2014;**156**(1-2):20–44.
61. Nielsen R, Pedersen TA, Hagenbeek D, Moulos P, Siersbaek R, Megens E, Denissov S, Børgesen M, Francoijs KJ, Mandrup S, Stunnenberg HG. Genome-wide profiling of PPARgamma:RXR and RNA polymerase II occupancy reveals temporal activation of distinct metabolic pathways and changes in RXR dimer composition during adipogenesis. *Genes Dev*. 2008;**22**(21):2953–2967.
62. Gupta RK, Arany Z, Seale P, Mepani RJ, Ye L, Conroe HM, Roby YA, Kulaga H, Reed RR, Spiegelman BM. Transcriptional control of preadipocyte determination by Zfp423. *Nature*. 2010; **464**(7288):619–623.
63. Jimenez MA, Akerblad P, Sigvardsson M, Rosen ED. Critical role for Ebf1 and Ebf2 in the adipogenic transcriptional cascade. *Mol Cell Biol*. 2007;**27**(2):743–757.
64. Vishvanath L, MacPherson KA, Hepler C, Wang QA, Shao M, Spurgin SB, Wang MY, Kusminski CM, Morley TS, Gupta RK. Pdgfrβ+ mural preadipocytes contribute to adipocyte hyperplasia induced by high-fat-diet feeding and prolonged cold exposure in adult mice. *Cell Metab*. 2016;**23**(2):350–359.
65. Daniel B, Nagy G, Hah N, Horvath A, Czimmerer Z, Poliska S, Gyuris T, Keirsse J, Gysemans C, Van Ginderachter JA, Balint BL, Evans RM, Barta E, Nagy L. The active enhancer network operated by liganded RXR supports angiogenic activity in macrophages. *Genes Dev*. 2014;**28**(14):1562–1577.
66. Matsumura Y, Nakaki R, Inagaki T, Yoshida A, Kano Y, Kimura H, Tanaka T, Tsutsumi S, Nakao M, Doi T, Fukami K, Osborne TF, Kodama T, Aburatani H, Sakai J. H3K4/H3K9me3 bivalent chromatin domains targeted by lineage-specific DNA methylation pauses adipocyte differentiation. *Mol Cell*. 2015;**60**(4):584–596.
67. Wang L, Jin Q, Lee JE, Su IH, Ge K. Histone H3K27 methyltransferase Ezh2 represses Wnt genes to facilitate adipogenesis. *Proc Natl Acad Sci USA*. 2010;**107**(16):7317–7322.
68. Yi SA, Um SH, Lee J, Yoo JH, Bang SY, Park EK, Lee MG, Nam KH, Jeon YJ, Park JW, You JS, Lee SJ, Bae GU, Rhie JW, Kozma SC, Thomas G, Han JW. S6K1 phosphorylation of H2B mediates EZH2 trimethylation of H3: a determinant of early adipogenesis. *Mol Cell*. 2016;**62**(3):443–452.
69. Hemming S, Cakouros D, Isenmann S, Cooper L, Menicanin D, Zannettino A, Gronthos S. EZH2 and KDM6A act as an epigenetic switch to regulate mesenchymal stem cell lineage specification. *Stem Cells*. 2014;**32**(3):802–815.
70. Wei Y, Chen YH, Li LY, Lang J, Yeh SP, Shi B, Yang CC, Yang JY, Lin CY, Lai CC, Hung MC. CDK1-dependent phosphorylation of EZH2 suppresses methylation of H3K27 and promotes osteogenic differentiation of human mesenchymal stem cells. *Nat Cell Biol*. 2011;**13**(1):87–94.
71. Hu L, Yang G, Hägg D, Sun G, Ahn JM, Jiang N, Ricupero CL, Wu J, Rodhe CH, Ascherman JA, Chen L, Mao JJ. IGF1 promotes adipogenesis by a lineage bias of endogenous adipose stem/progenitor cells. *Stem Cells*. 2015;**33**(8):2483–2495.
72. Claussnitzer M, Dankel SN, Kim KH, Quon G, Meuleman W, Haugen C, Glunk V, Sousa IS, Beaudry JL, Puviindran V, Abdennur NA, Liu J, Svensson PA, Hsu YH, Drucker DJ, Mellgren G, Hui CC, Hauner H, Kellis M. FTO obesity variant circuitry and adipocyte browning in humans. *N Engl J Med*. 2015; **373**(10):895–907.
73. Birsoy K, Chen Z, Friedman J. Transcriptional regulation of adipogenesis by KLF4. *Cell Metab*. 2008;**7**(4):339–347.
74. Wu H, Gordon JA, Whitfield TW, Tai PW, van Wijnen AJ, Stein JL, Stein GS, Lian JB. Chromatin dynamics regulate mesenchymal stem cell lineage specification and differentiation to osteogenesis. *Biochim Biophys Acta*. 2017;**1860**(4):438–449.
75. Juan AH, Wang S, Ko KD, Zare H, Tsai PF, Feng X, Vivanco KO, Ascoli AM, Gutierrez-Cruz G, Krebs J, Sidoli S, Knight AL, Pedersen RA, Garcia BA, Casellas R, Zou J, Sartorelli V. Roles of H3K27me2 and H3K27me3 examined during fate specification of embryonic stem cells. *Cell Rep*. 2016;**17**(5):1369–1382.
76. Guelen L, Pagie L, Brasset E, Meuleman W, Faza MB, Talhout W, Eussen BH, de Klein A, Wessels L, de Laat W, van Steensel B. Domain organization of human chromosomes revealed by mapping of nuclear lamina interactions. *Nature*. 2008;**453**(7197):948–951.
77. Attina TM, Hauser R, Sathyanarayana S, Hunt PA, Bourguignon JP, Myers JP, DiGangi J, Zoeller RT, Trasande L. Exposure to

endocrine-disrupting chemicals in the USA: a population-based disease burden and cost analysis. *Lancet Diabetes Endocrinol*. 2016;**4**(12):996–1003.
78. Trasande L, Zoeller RT, Hass U, Kortenkamp A, Grandjean P, Myers JP, DiGangi J, Bellanger M, Hauser R, Legler J, Skakkebaek NE, Heindel JJ. Estimating burden and disease costs of exposure to endocrine-disrupting chemicals in the European Union. *J Clin Endocrinol Metab*. 2015;**100**(4):1245–1255.
79. Legler J, Fletcher T, Govarts E, Porta M, Blumberg B, Heindel JJ, Trasande L. Obesity, diabetes, and associated costs of exposure to endocrine-disrupting chemicals in the European Union. *J Clin Endocrinol Metab*. 2015;**100**(4):1278–1288.
80. Bowers RR, Temkin AM, Guillette LJ, Baatz JE, Spyropoulos DD. The commonly used nonionic surfactant Span 80 has RXRα transactivation activity, which likely increases the obesogenic potential of oil dispersants and food emulsifiers. *Gen Comp Endocrinol*. 2016;**238**:61–68.
81. Pereira-Fernandes A, Vanparys C, Vergauwen L, Knapen D, Jorens PG, Blust R. Toxicogenomics in the 3T3-L1 cell line, a new approach for screening of obesogenic compounds. *Toxicol Sci*. 2014; **140**(2):352–363.
82. Bastos Sales L, Kamstra JH, Cenijn PH, van Rijt LS, Hamers T, Legler J. Effects of endocrine disrupting chemicals on in vitro global DNA methylation and adipocyte differentiation. *Toxicol In Vitro*. 2013;**27**(6):1634–1643.
83. Taxvig C, Dreisig K, Boberg J, Nellemann C, Schelde AB, Pedersen D, Boergesen M, Mandrup S, Vinggaard AM. Differential effects of environmental chemicals and food contaminants on adipogenesis, biomarker release and PPARγ activation. *Mol Cell Endocrinol*. 2012;**361**(1-2):106–115.
84. Kassotis CD, Masse L, Kim S, Schlezinger JJ, Webster TF, Stapleton HM. Characterization of adipogenic chemicals in three different cell culture systems: implications for reproducibility based on cell source and handling. *Sci Rep*. 2017;**7**:42104.
85. AlSudais H, Aabed K, Nicola W, Dixon K, Chen J, Li Q. Retinoid X receptor-selective signaling in the regulation of Akt/protein kinase B isoform-specific expression. *J Biol Chem*. 2016;**291**(6): 3090–3099.
86. Le May M, Mach H, Lacroix N, Hou C, Chen J, Li Q. Contribution of retinoid X receptor signaling to the specification of skeletal muscle lineage. *J Biol Chem*. 2011;**286**(30):26806–26812.
87. Mark M, Ghyselinck NB, Chambon P. Function of retinoic acid receptors during embryonic development. *Nucl Recept Signal*. 2009;**7**:e002.
88. Froment P. PPARs and RXRs in male and female fertility and reproduction. *PPAR Res*. 2008;**2008**:637490.